HHS Public Access

Author manuscript

Phys Med Biol. Author manuscript; available in PMC 2016 December 08.

Published in final edited form as:

Phys Med Biol. 2015 September 07; 60(17): 6701–6718. doi:10.1088/0031-9155/60/17/6701.

Cherenkov radiation fluence estimates in tissue for molecular imaging and therapy applications

Adam K. Glaser[1], **Rongxiao Zhang**[2], **Jacqueline M. Andreozzi**[1], **David J. Gladstone**[1,3,4], and **Brian W. Pogue**[1,2]

Adam K. Glaser: Adam.K.Glaser@dartmouth.edu; Brian W. Pogue: Brian.W.Pogue@dartmouth.edu

[1]Thayer School of Engineering, Dartmouth College, Hanover, New Hampshire 03755

[2]Department of Physics and Astronomy, Dartmouth College, Hanover, New Hampshire 03755

[3]Norris Cotton Cancer Center, Lebanon, New Hampshire 03756

[4]Geisel School of Medicine, Dartmouth College, Hanover, New Hampshire 03755

Abstract

Cherenkov radiation has recently emerged as an interesting phenomenon for a number of applications in the biomedical sciences. Its unique properties, including broadband emission spectrum, spectral weight in the ultraviolet and blue wavebands, and local generation of light within a given tissue, have made it an attractive new source of light within tissue for molecular imaging and phototherapy applications. While several studies have investigated the total Cherenkov light yield from radionuclides in units of [photons/decay], further consideration of the light propagation in tissue is necessary to fully consider the utility of this signal *in vivo*. Therefore, to help further guide the development of this novel field, quantitative estimates of the light fluence rate of Cherenkov radiation from both radionuclides and radiotherapy beams in a biological tissue are presented for the first time. Using Monte Carlo simulations, these values were found to be on the order of 0.01 – 1 nW/cm^2 per MBq/g for radionuclides, and 1 – 100 μW/cm^2 per Gy/sec for external radiotherapy beams, dependent on the given waveband, optical properties, and radiation source. For phototherapy applications, the total light fluence was found to be on the order of nJ/cm^2 for radionuclides, and mJ/cm^2 for radiotherapy beams. The results indicate that diagnostic potential is reasonable for Cherenkov excitation of molecular probes, but phototherapy may remain elusive at such exceedingly low fluence values. The simulation tools of this study are available upon request.

1. Introduction

In recent years there has been a growing interest in biophotonic applications of Cherenkov radiation, a form of light emission that occurs when a charged particle exceeds the local speed of light in a dielectric medium (Čerenkov, 1937). To date, these applications have included small animal imaging and tomography of radionuclide distributions and kinetics (Robertson et al., 2009, Hu et al., 2010, Li et al., 2010, Spinelli et al., 2010, Mitchell et al., 2011, Boschi et al., 2011), clinical imaging of ^{18}F-FDG in human patients (Holland et al., 2011, Thorek et al., 2014), intraoperative imaging (Holland et al., 2011, Thorek et al., 2012, Liu et al., 2012, Carpenter et al., 2014), as well as dosimetric imaging during external beam

radiation therapy and brachytherapy (Glaser et al., 2013a, Glaser et al., 2013b, Glaser et al., 2013d, Glaser et al., 2014, Zhang et al., 2013a, Zhang et al., 2013c, Zhang et al., 2013b, Jarvis et al., 2014, Lohrmann et al., 2015). While all of these studies have appreciated the inherently weak intensity of this form of light emission, there have been limited attempts at absolute quantification of the light fluence of Cherenkov radiation for each of these applications. Simple experimental measurements have suggested that the light fluence from radiotherapy beams is on the order of [nW/cm^2], and no light fluence measurements have been reported for radionuclides in mammalian tissue (Axelsson et al., 2011, Glaser et al., 2012). Previous studies have explored the light production of a number of radionuclides in [photons/decay], but the subsequent optical light transport was not considered, an important additional step in estimating the light fluence for biomedical applications (Beattie et al., 2012, Gill et al., 2015).

Estimates of this quantity are particularly important in guiding the development of future imaging systems and biophotonics applications utilizing Cherenkov radiation, particularly with the emerging interest in using Cherenkov radiation for low fluence threshold phototherapy (Ran et al., 2012, Gonzales et al., 2014, Kotagiri et al., 2015, Hartl et al., 2015). Herein we develop a robust and flexible methodology for modeling both the radiation and optical light transfer for quantifying the light fluence of Cherenkov radiation from any radiation source, spatial distribution, and optical properties, and provide example estimates for a number of relevant radionuclides and radiotherapy beams using a recently developed and validated Monte Carlo package for the simulation of radiation-induced light transport in biological media (Glaser et al., 2013c). The simulation results of this study are available upon request.

2. Materials and methods

2.1 Simulation methodology

Monte Carlo simulations were run using the Geant4 Architecture for Medically-oriented Simulations (GAMOS) tissue-optics plugin (Agostinelli et al., 2003, Arce et al., 2008, Glaser et al., 2013c). In the case of radionuclides, decays were modeled using the radioactive decay physics process, which properly models all disintegrations specific to each radionuclide. In total, ten radionuclides were modeled, including ^{225}Ac, ^{11}C, ^{64}Cu, ^{18}F, ^{68}Ga, ^{131}I, ^{13}N, ^{15}O, ^{90}Y, and ^{89}Zr. In each simulation, all disintegrations were initiated at the origin of the simulation in a soft tissue volume of refractive index $n = 1.37$, and the optical fluence was recorded in spherical coordinates at radial distances of 0 – 2 cm in 0.1 mm increments from the origin for a waveband of 400 – 700 nm. The resulting radial fluence therefore represents the Green's function of Cherenkov light emission in a medium with given optical scattering and absorption properties. The Green's function for light fluence, G_L (r, μ_a, μ_s) [photons/cm^2/particle], normalized per decay, was simulated as a function of optical scattering and absorption for a number of discrete, spectrally constant values, varied logarithmically, μ_a ranging from zero and 0.00001 up to 100] mm^{-1} and μ_s from 1 up to 250.0 mm^{-1}. For all simulations the anisotropy was fixed at an average cosine value, $g = 0.9$, to estimate what the reduced scattering coefficient, μ_s', would be.

In the case of radiotherapy beams, x-ray photon and electron beams were modeled using Varian proprietary phase space files (available at myvarian.com). Although these phase space files are recorded above the jaws, the spectrum of all particles was calculated and then used as the input spectrum for a pencil beam incident on a soft tissue volume of refractive index $n = 1.37$. For x-ray photons, beam energies of 4, 6, 8, 10, and 15 MV were modeled, and for electrons beam, energies of 6, 9, 12, 15, and 18 MeV were modeled. The light fluence due to the pencil beams was recorded in cylindrical coordinates at radial positions of 0 – 2 cm in 0.1 mm increments from the origin, and depths of 0 – 10 cm in 0.1 mm increments from the tissue surface. The Green's function for light fluence, $G_L(r, z, \mu_a, \mu_s)$ [photons/cm^2/particle], normalized per incident particle, was simulated as a function of the same optical scattering, absorption, and anisotropy as for the radionuclides. In addition, the Green's function for dose deposition, $G_D(r, z)$ [Gy/particle], was recorded. The dose deposition, $G_D(r)$ [Gy/particle], was also recorded for ^{90}Y. Note that the Green's functions for dose deposition are independent of optical properties. Representative geometries for both simulations are shown in Figure 1.

2.2 Convolution

To calculate quantitative light fluence fields for finite sized radiotherapy beam or radionuclide distribution, either two-dimensional (2D) convolution over the uniform circular beam field size or three-dimensional (3D) convolution over a uniform spherical distribution was performed. In the case of 2D convolution, the convolution light fluence distribution, $C_L(r, z, \mu_a, \mu_s)$ [photons/cm^2/(particles/cm^2)], can be calculated from Eq. (1) as

$$C_L(r,z,\mu_a,\mu_s)=\int_0^{\infty} S(r')r'\left[\int_0^{2\pi} G_L\left(\sqrt{r^2+r'^2-2rr'\cos\theta'},z,\mu_a,\mu_s\right)d\theta'\right]dr' \quad (1)$$

where $S(r')$ [particles/cm^2] is the source distribution, uniform for r' from 0 to R for a circle of radius R. A similar expression can be derived for 3D convolution, where the convolved light fluence distribution, $C_L(r, \mu_a, \mu_s)$ [photons/cm^2/(particle/cm^3)], can be calculated from Eq. (2) as

$$C_L(r,\mu_a,\mu_s)=\int_0^{\infty} S(r')r'^2\left[\int_0^{2\pi}\int_0^{\pi} G_L\left(\sqrt{r^2+r'^2-2rr'\cos\theta'}\cos\varphi',\mu_a,\mu_s\right)\sin\theta'\,d\theta'\,d\varphi'\right]dr' \quad (2)$$

where $S(r')$ [cm^{-3}], the source distribution is uniform for r' from 0 to R for a sphere of radius R. Similarly, the convolved dose distributions, $C_D(r, z, \mu_a, \mu_s)$ [Gy/(particles/cm^2)] and $C_D(r, \mu_a, \mu_s)$ [Gy/(particles/cm^3)] can be calculated from Eqs. (3) and (4) as

$$C_D(r,z)=\int_0^{\infty} S(r')r'\left[\int_0^{2\pi} G_D\left(\sqrt{r^2+r'^2-2rr'\cos\theta'},z\right)d\theta'\right]dr' \quad (3)$$

$$C_D(r)=\int_0^{\infty} S(r')r'^2\left[\int_0^{2\pi}\int_0^{\pi} G_D\left(\sqrt{r^2+r'^2-2rr'\cos\theta'}\cos\varphi'\right)\sin\theta' d\theta' d\varphi'\right]dr' \quad (4)$$

For this study, R was chosen to be 2.5 mm for the 2D and 3D convolution.

2.3 Optical properties

To model the spectral fluence of Cherenkov radiation in a generic tissue, the lookup table of convolved light fluence maps as a function of optical scattering and absorption were interpolated using a parametric mapping of optical properties to wavelength space. To generate biologically relevant scattering and absorption coefficients, a methodology analogous to Jacques *et. al.* was utilized (Jacques, 2013). Here, the reduced scattering coefficient, $\mu_s'(\lambda)$ [mm^{-1}], is empirically modeled as a superposition of Rayleigh and Mie scattering

$$\mu_s'(\lambda)=a\left[f_{\mathrm{Ray}}\left(\frac{\lambda}{500[\mathrm{nm}]}\right)^{-4}+(1-f_{\mathrm{Ray}})\left(\frac{\lambda}{500[\mathrm{nm}]}\right)^{-b_{\mathrm{Mie}}}\right] \quad (5)$$

where a is the scatter amplitude [mm^{-1}], f_{Ray} [arb. u.] is the component fraction of Rayleigh scattering, and b_{Mie} [arb. u.] is the scatter power. The scattering coefficient, $\mu_s(\lambda)$ [mm^{-1}] can then be calculated as

$$\mu_s(\lambda)=\frac{\mu_s'}{(1-g)} \quad (6)$$

where g is the scattering anisotropy.

Similarly, the absorption coefficient, $\mu_a(\lambda)$ [mm^{-1}], can be calculated as a superposition of absorption due to oxygenated hemoglobin, $\mu_{a,oxy}$ [mm^{-1}], deoxygenated hemoglobin, $\mu_{a,deoxy}$ [mm^{-1}], water, $\mu_{a,water}$ [mm^{-1}], and fat, $\mu_{a,fat}$ [mm^{-1}], where

$$\mu_a(\lambda)=BS\mu_{a,\mathrm{oxy}}+B(1-S)\mu_{a,\mathrm{deoxy}}+W\mu_{a,\mathrm{water}}+F\mu_{a,\mathrm{fat}} \quad (7)$$

B [%] is the volume fraction of blood, S [%] is the oxygen saturation, W [%] is the volume fraction water, and F [%] is the volume fraction fat. The absorption coefficient of

oxygenated and deoxygenated hemoglobin can be further decomposed into Eq. (8), which relates the blood concentration, C_{HGb} [μM]

$$\mu_{a,\mathrm{oxy/deoxy}}=\ln(10)\varepsilon_{\mathrm{oxy/deoxy}}C_{m,HGb} \quad (8)$$

where $\varepsilon_{oxy/deoxy}$ [$mm^{-1}μM^{-1}$] is the extinction coefficient of whole blood. Based on these empirical equations, relevant values from the literature were used to construct 40 generic breast tissues, based upon 8 unique scattering coefficients and 5 unique absorption coefficients. The scattering parameters and absorption parameters are summarized in Tables 1 and 2. The calculated scattering and absorption coefficients (mean and range) are shown in Figure 2.

2.3 Spectral scaling

As described in Section 2.1, the fluence estimates were for a wide waveband, 400 – 700 nm. To calculate the Cherenkov light emission in any arbitrary waveband, the Frank-Tamm formula can be used, which describes the total emission, N[photons] over a path length, dx [nm],

$$N=\int 2\pi\alpha({\lambda_1}^{-1}-{\lambda_2}^{-1})\left(1-\frac{1}{\beta^2n^2}\right)dx \quad (9)$$

where α [arb. u.] is the fine structure constant, β [arb. u.] is the ratio of the particle velocity to the speed of light in vacuum, and λ_1 and λ_2 describe the waveband of interest in [nm]. Therefore, based upon the emission between 400 – 700 nm, the emission at any arbitrary waveband can be calculated as a ratio of the two wavebands. Using the optical properties defined in Section 2.2, the spectrally dependent light fluence maps, $\varphi(r, \lambda_3 \le \lambda \le \lambda_4)$ [photons/cm^2/(particles/cm^3)/nm] and $\varphi(r, z, \lambda_3 \le \lambda \le \lambda_4)$ [photons/cm^2/(particles/cm^2)/nm] were numerically calculated between 250 – 850 nm in 1 nm increments in Eq. (10) and (11) as

$$\varphi(r,\lambda_3\le\lambda\le\lambda_4)=C_L(r,\overline{\mu_a},\overline{\mu_s})\left(\frac{{\lambda_3}^{-1}-{\lambda_4}^{-1}}{{\lambda_1}^{-1}-{\lambda_2}^{-1}}\right) \quad (10)$$

$$\varphi(r,z,\lambda_3\le\lambda\le\lambda_4)=C_L(r,z,\overline{\mu_a},\overline{\mu_s})\left(\frac{{\lambda_3}^{-1}-{\lambda_4}^{-1}}{{\lambda_1}^{-1}-{\lambda_2}^{-1}}\right) \quad (11)$$

where $\overline{\mu_a}[\mathrm{mm}^{-1}]$ and $\overline{\mu_a}[\mathrm{mm}^{-1}]$ are the average absorption and scattering coefficients between λ_3 and λ_4 [nm], and λ_1 and λ_2 were 400 and 700 nm respectively.

2.4 Fluence and fluence rates

Eqs. (10) and (11) represent the specific fluence in units of [photons/cm^2/nm] per [particles/cm^3] for radionuclides, corresponding to the 3D convolution over the distribution volume, or [particles/cm^2] for radiotherapy beams corresponding to the 2D convolution over the field size. For a given radionuclide, the fluence rate [W/cm^2/nm] can be calculated as

$$\Phi(r,\lambda_3\le\lambda\le\lambda_4)=\frac{A}{V}\varphi(r,\lambda_3\le\lambda\le\lambda_4) \quad (12)$$

where A is the activity of the radionuclide [Bq] per unit volume, V [cm^3]. This quantity can also be equivalently expressed per unit mass if the density of the medium is known. For these simulations in soft tissue, under the assumption that the density of tissue is approximately 1 g/cm^3 Eq. (12) is consistent per cm^3 or g. To calculate the total fluence [J/cm^2/nm] Eq. (12) can be integrated in time as

$$\phi(r,\lambda_3\le\lambda\le\lambda_4)=\frac{1}{\alpha}\Phi(r,\lambda_3\le\lambda\le\lambda_4) \quad (13)$$

where α [sec^{-1}] is the decay constant of the radionuclide. Equivalently, the total fluence can be calculated if the number of radioactive decays per unit volume is known. In this case the expression becomes

$$\phi(r,\lambda_3\le\lambda\le\lambda_4)=\frac{N}{V}\varphi(r,\lambda_3\le\lambda\le\lambda_4) \quad (14)$$

where the unit of N is [particles]. For a given radiotherapy beam, the fluence rate [W/cm^2/nm] can be expressed as

$$\Phi(r,z,\lambda_3\le\lambda\le\lambda_4)=M(r,z)\frac{\varphi(r,z,\lambda_3\le\lambda\le\lambda_4)}{C_D(r,z)} \quad (15)$$

where M is the dose rate in [Gy/sec] at the given position (r, z) in the medium. Similarly, the total fluence [J/cm^2/nm] can be calculated by integrating in time, or simply multiplying by the delivered dose as

$$\phi(r,z,\lambda_3\le\lambda\le\lambda_4)=D(r,z)\frac{\varphi(r,z,\lambda_3\le\lambda\le\lambda_4)}{C_D(r,z)} \quad (16)$$

where D is the delivered dose in [Gy] at the given position (r, z). Note for ^{90}Y only, the fluence rate was also evaluated as a function of dose rate with Eq. (15) and as a function of radius, r, instead of both r, and depth, z.

2.5 Estimates of fluence rate for radionuclides and radiotherapy beams

To simplify the presentation of the Monte Carlo results, the fluence rates given by Eqs. (12) and (15) were calculated at a single spatial location. In the case of the radionuclides, the fluence rate is approximately constant inside the sphere of radius R due to the convolution performed in Eq. (1). Similarly, for radiotherapy beams, the fluence rate was evaluated at the (r, z) location where the dose given by Eq. (3) reaches a maximum. For both x-ray and electron beams, this occurs at $(0, d_{max})$ where d_{max}[cm] is known as the depth of maximum dose. Therefore the resulting fluence rate, $\Phi(\lambda)$, [W/cm^2/nm] is only a function of wavelength. In addition, no assumptions were made about A/V [Bq/cm^3 or Bq/g] or M [Gy/sec], and the results were calculated per unit activity per unit volume, or mass and per unit dose rate.

2.6 Dependence on refractive index

Due to the fact that Cherenkov light emission is a function of refractive index, see Eq. (9), the fluence rate for all radionuclides and radiotherapy beams was also recorded for refractive indices ranging from 1.3 – 1.6, in steps of 0.01. This dependence arises from the fact that the threshold energy for light emission is refractive index dependent, e.g. in water (n = 1.33) charged particles must have an energy greater than ~264 keV, whereas in plastic (n = 1.59) this threshold drops to ~146 keV. Therefore, using ^{18}F as an example, a positron emitted at an energy of 633 keV would reduce in energy linearly (under the assumption of linear energy transfer), and emit Cherenkov radiation for ~58% of its track length water, or ~77% in the case of plastic.

It should be noted that this is a larger factor for particle emissions close to the threshold energy, whereas emissions in the MeV range are largely unaffected. For these simulations, only one representative set of optical properties was necessary, and therefore the following values were used: μ_s = 10.0 mm^{-1}, g = 0.9, μ_a = 0.1 mm^{-1}. The resulting fluence rates were normalized at a refractive index value of n = 1.37 (used for all other simulations) to calculate a refractive index factor

$$K = \frac{\Phi(n)}{\Phi(n=1.37)} \quad (17)$$

2.7 Experimental validation

In an attempt to experimentally validate the simulated values by order of magnitude, the Cherenkov light emission fluence rate of a 6 MV x-ray beam from a Varian 2100C/D Linac (Varian Medical Systems, Palo Alto, CA) was measured. An optical phantom consisting of phosphate buffered solution and 1% v/v Intralipid (Sigma Aldrich, St. Loius, MO) was created, and a 635 nm laser (Thorlabs, Newton, NJ) was used to illuminate the top of the phantom. On the left and right sides of the phantom respectively, a power meter (Thorlabs, Newton, NJ) and detection system consisting of a fiber (Zlight, Latvia), spectrograph (SpectraPro, Princeton Instruments, Acton, MA), and CCD (PI-MAX3 Unigen2, Princeton Instruments, Acton, MA) cooled to −25 °C were used to record data from the illuminating laser. The power meter reading [W/cm^2] was compared to the detection system reading

[counts/sec] to obtain a conversion factor between the two quantities at the 635 nm laser wavelength. This factor, S, [W/cm^2/(counts/sec)] was calculated as

$$S=\frac{\Phi_M[635\ \mathrm{nm}]}{\frac{\sum_\lambda I}{t}} \quad (18)$$

where Φ_M[W/cm^2] is the power meter reading, $\Sigma_\lambda I$[counts] represents the total number of counts recorded by the fiber system, and t[sec] is the total exposure time of the spectral measurement. The power meter and laser were then removed, and a 5×5 cm radiation beam was delivered to the phantom at a dose rate of 6 Gy/min or 0.1 Gy/sec, with the fiber submerged at a depth of 4 cm in the phantom, and the fiber system gated to the Linac pulse with 200 on chip accumulations and a gate width of 3.25 μs (Glaser et al., 2012). The recorded [counts/sec] with the tip of the optical fiber exposed (representing signal induced in the optical phantom superimposed with signal induced in the fiber itself), and covered with black tape (representing only the Cherenkov signal induced in the fiber itself) were measured, and the difference of the two measurements (representing only the signal due to the optical phantom) was calibrated to $\Phi'_X(\lambda_1 \le \lambda \le \lambda_2)[\mathrm{W/cm^2/nm}]$ using the following procedure equation

$$\Phi'_X(\lambda_1 \le \lambda \le \lambda_2)=\frac{s}{\lambda_2-\lambda_1}\times\frac{I(\lambda_1 \le \lambda \le \lambda_2)}{t}\times\frac{635\ \mathrm{nm}}{\bar{\lambda}[\mathrm{nm}]} \quad (19)$$

where S[W/cm^2/(counts/sec)] was given by Eq. (18), $\lambda_2 - \lambda_1$ [nm] is the discrete waveband designated by the spectrograph, $I(\lambda_1 \le \lambda \le \lambda_2)$ [counts] is the intensity collected in this waveband, calibrated for spectral sensitivity relative to 635 nm using a white light calibration source (IntelliCall Intensity Calibration Lamp, Princeton Instruments, Acton, MA) t[sec] is the exposure time for the gated measurement, and the third term accounts for the wavelength dependence of photon energy, at $\bar{\lambda}$[nm], the mean wavelength between λ_1 and λ_2 normalized to a value of 1.0 at 635 nm where the power meter calibration measurement was recorded. This quantity represents the fluence rate of a gated measurement. However, the continuous wave fluence rate, $\Phi_X(\lambda_1 \le \lambda \le \lambda_2)$ [W/cm^2/nm] corresponding to a non-gated measurement could be calculated as

$$\Phi_X(\lambda_1 \le \lambda \le \lambda_2)=\Phi'_X \times f \times w \quad (20)$$

where f is the pulse frequency ~ 360 [Hz] and w is the gate width of 3.25 μs. Therefore, the continuous wave fluence rate is ~ 1000× weaker than the gated measurement, as shown previously (Glaser et al., 2012). The experimental fluence rate given by Eq. (20) was compared to the simulated fluence rate given by Eq. (15) at the experimental measured position of (0, 4 cm). The experimental geometry is shown in Figure 3.

3. Results

3.1 Simulation results

Representative results for the fluence rate of ^{18}F and a 6 MV x-ray photon beam for all 40 optical property pairs both with and without optical absorption are shown in Figure 4.

The results in Figure 4 are representative spectral results for the radionuclide and radiotherapy beam cases. The relative spectral shape of the results is independent of the radiation source (radionuclide type or radiotherapy beam energy) and depends only upon the optical scattering and absorption. Therefore, for both the optical scattering and absorption, as well as the scattering only simulations, the percent contribution of each waveband from 250 – 850 nm in 100 nm bins are presented in Table 3.

The full results for fluence rates integrated between 250 – 850 nm are shown in Figure 5.

The results for the fluence rate as function of refractive index for both the radionuclides as well as the external radiotherapy beams are shown in Figure 6. For comparison, the result for ^{90}Y is plotted in both Figure 6(a) and 6(b).

3.2 Experimental results

The experimentally measured fluence rate as a function of wavelength, given by Eq. (20) is plotted in Figure 7 in comparison to Eq. (15) for a 6 MV external radiotherapy beam for a 1% v/v Intralipid phantom. The mean measurement (solid blue line), as well as the uncertainty in the measurement as calculated by the standard deviation in each waveband over 20 successive measurements (shaded region) is shown in comparison to the predicted fluence rate from the Monte Carlo simulations (solid yellow line). The additional lines (dotted gray) represent the simulated fluence multiplied by a factor of 2, 3, 4, and 5 respectively.

4. Discussion

While previous studies have reported quantitative estimates of the total Cherenkov light yield from radionuclides in units of [photons/decay], the results in this study aim to quantify both the generation and transport of this light in a biological tissue by reporting the light fluence [J/cm^2] and fluence rate [W/cm^2] from both radionuclides and radiotherapy beams. Due to the broadband, white-light nature of this emission, optical properties of generic breast tissue from a number of sources in the literature were evaluated. In the case of radionuclides, the fluence rate was calculated as a function of activity per unit mass [MBq/g] and in the case of external radiotherapy beams, the fluence rate was calculated as a function of dose rate [Gy/sec]. In general, the fluence rate between 250 – 850 nm from radionuclides was found to be on the order of 0.3 – 30 fW/cm^2/(MBq/g). Similarly, the fluence rate from external radiotherapy beams was found to be on the order of 300 – 500 nW/cm^2/(Gy/sec).

Despite the weighting of Cherenkov light emission in the ultraviolet and blue wavebands, due to the optical absorption of water, hemoglobin, and fat, the fluence rate was found to be strongest beyond 600 nm. However, an interesting characteristic of Cherenkov radiation is

its local generation inside a medium, as opposed to delivery of light inside a biological medium from an external light source. In the latter case, light reaching a region of interest within a medium is diffuse and is therefore heavily attenuated by the optical absorption of the tissue. In the case of Cherenkov radiation, light may be generated inside a given cell and experience little optical absorption at the microscopic level. Therefore, light fluence rate estimates were also computed in the presence of optical scattering, but in the absence of optical absorption. In this case, the fluence rate of radionuclides was found to be on the order of 5 – 500 fW/cm^2/(MBq/g) and that of external radiotherapy beams was on the order of 4,000 – 8,000 nW/cm^2/(Gy/sec). Therefore, in the absence of optical absorption the fluence rate of Cherenkov light emission from either radiation source is increased by ~ 1 – 2 orders of magnitude, and the overall limits for the expected fluence rate is 0.3 – 500 fW/cm^2/(MBq/g) for radionuclides, or 300 – 8000 nW/cm^2/(Gy/sec). In both cases, the percentage variation due to optical properties is comparable, but simply appears larger in Figure 5 due to the log display of a multiplicative rather than additive quantity.

As has been reported previously, for radionuclides a strong variation in fluence rate exists between different radionuclides due to the different particle emission energies. For example, in the prescence of optical absorption the fluence rate of ^{90}Y was found to be ~35 fW/cm^2/(MBq/g), while the fluence rate of ^{11}C was found to be ~4 fW/cm^2/(MBq/g). These results are consistent with the a recent report by Gill *et al.*, where the total Cherenkov light yield of ^{90}Y was found to be 47.3 photons/decay while the total light yield of ^{11}C was calculated to be 6.87 photons/decay (Gill et al., 2015). A comprehensive comparison between the results obtained in this study and Gill *et. al.*, are presented in Figure 8. Due to the fact that the results in this study were calculated for a waveband of 250 – 850 nm, whereas the previous study examined 400 – 800 nm, the results were scaled to match the 250 – 850 nm waveband using an equation analogous to Eqs. (10) and (11). In addition, the slope of the linear fitting lines between the fluence rate, Φ, and light yield, N[photons/decay], presented by Gill *et. al.* are displayed. As can be seen, the results are consistent for each radiotracer, and the ratio is ~4.7 in the absence of optical absorption, and ~0.3 in the presence of optical absorption. These results demonstrate the agreement between the results of these two studies, as well the significant role that optical properties may play in modulating the fluence and fluence rate which arise from the total Cherenkov light yields calculated by Gill *et. al.* in [photons/decay].

When analyzed as a function of dose rate, the fluence rate from a ^{90}Y source is comparable to external radiotherapy beams. In contrast to radionuclides, the observed variation in fluence rate as a function of energy was minimal for radiotherapy beams due to the normalization as a function of dose rate, i.e. the number of Cherenkov photons generated per unit dose for any radiotherapy beam does not change dramatically. The dependence of the fluence rate on refractive index was found to be within 0 – 4 for radionuclides, where radionuclides with particle emission energies closest to the threshold energy condition for Cherenkov light emission were the most sensitive. These results are also consistent with the result report by Gill *et. al.*, where the total Cherenkov light yield of ^{18}F was found to vary 1.0 – 3.5 (between 1.33 and 1.49 normalized to 1.0 at 1.33), whereas in this study, the dependence of ^{18}F was found to be 0.66 – 2.25 (between 1.33 and 1.49 normalized to 1.0 at 1.37) or 1.0 – 3.4 when normalized similarly at 1.33.

On the other hand, the factor was found to be only 0 – 1.5 for radiotherapy beams due to the high energy of particles used in external beam radiotherapy. Therefore, for the fluence rate ranges listed above, decreases or increases in the refractive index in the medium could modulate the values by 0 – 4 in the case of radionuclides, and 0 – 1.5 in the case of radiotherapy beams. Finally, while the majority of the results presented in this paper are driven by Monte Carlo simulations, experimental validation of the fluence rate from a 6 MV external radiotherapy beam in an Intralipid phantom operating at a dose rate of 6 Gy/min was found to be within a factor of 2 – 3 of the expected simulation result, confirming the validity of the simulations to within an order of magnitude. In the case of radionuclides, estimates can be inferred from results of the IVIS-100 imaging system used throughout the majority of the relevant literature. For example, for a tail vein injection of 8 μCi (~0.3 MBq) of ^{90}Y-AABD in a mouse model, the collected signal was ~30,000 [photons/sec/cm^2/sr]. Assuming a spectral sensitivity of the IVIS-100 imaging system of approximately 400 – 800 nm, (600 nm mean wavelength), this value can be converted to a fluence rate value of 2.3 fW/cm^2/sr. This is in comparison to the simulation results of this study, where if we assume the a tissue tracer concentration of 0.003 – 0.03 MBq/g (equivalent to 1 – 10% ID/g), and normalized the results by 4π sr, the fluence rate between 400 – 800 nm in the presence of optical absorption would be ~100 – 1000 fW/cm^2/sr. This is simply a first order approximation, yet the agreement is reasonable due to the fact that the simulation results presented in this study represent the internal fluence rate, whereas the experimental measurements of an IVIS-100 imaging system represent the fluence rate emanating from the surface of an animal, which is expected to be orders of magnitude lower due to optical attenuation of the Cherenkov light over its propagation to the animal surface. The magnitude of this attenuation would be governed by the optical properties of the animal, a representative plot for the simulated fluence rate from a uniformly distributed spheroid of ^{90}Y of radius 0.25 cm and tissue tracer concentration of 0.003 MBq/g between 400 – 800 nm averaged across all of the optical properties combinations used in this study (including absorption) is shown in Figure 9 to demonstrate the attenuation of the Cherenkov light signal with radial distance. As expected the signal is attenuated by several orders of magnitude over just a few mm.

4.1 Molecular imaging with Cherenkov radiation

For molecular imaging applications, the fluence rate is the primary quantity of interest. In the case of radionuclides, the results of are presented per tissue activity concentration. This quantity is both organ and radionuclide dependent, but as an example, the myocardium tissue activity concentration of ^{18}F has been estimated to be in the range of 1 – 10 MBq/g (Kudo et al., 2002). Under these conditions, the local fluence rate of Cherenkov radiation would be ~0.3 – 300 fW/cm^2 in the presence of optical absorption, or ~5 – 5,000 fW/cm^2 in the absence of optical absorption, between 250 – 850 nm.

For radiotherapy beams, the dose rate is easily specified on a given treatment machine and can therefore be inserted directly into Eq. (15). For most modern linear accelerators, this range can be approximated as 1 – 10 Gy/min, although without a flattening filter dose rates can exceed 20 Gy/min. Therefore, for a 6 MV x-ray photon beam, the local Cherenkov

radiation fluence would be ~300 – 5,000 nW/cm^2 in the presence of optical absorption or ~300 – 80,000 nW/cm^2 in the absence of optical absorption between 250 – 850 nm.

These values could be further broken down into a specific waveband by using the percentages listed in Table 3, and scaled based upon the refractive index factor given in Figure 6. Imaging of these optical signals is achievable by using highly sensitive cameras, or long exposure times. In the case of radionuclides, this weak signal requires exposure times on the order of minutes, whereas this signal from radiotherapy beams can be captured in near real-time (Zhang et al., 2013b). So it is important to recognize that using these signals for molecular imaging is feasible, but typically would require some of the most sensitive measurements systems or cameras available.

4.2 Phototherapy with Cherenkov radiation

To calculate the total fluence delivered to tissue from a radionuclide, the fluence rate must be integrated in time, or more simply, the total number of radioactive decays per unit volume must be known. Calculation of these quantities has been studied previously for applications in radiation dosimetry of PET scans using the MIRD system (ICRP, 1988). Once again using ^{18}F as an example, the number of decays in each organ has been reported to be on the order of 100 – 100,00 decays per injected Bq. Using a conservative estimate of an organ volume of 10 cm^3, and a typical injected concentration of 370 MBq, the total fluence delivered within a representative organ would be ~3.5 – 3,500 nJ/cm^2 in the presence of optical absorption, or ~ 50 – 50,000 nJ/cm^2 in the absence of optical absorption, between 250 – 850 nm. Given the similar Cherenkov radiation fluence rates calculated for the various radionuclides presented in this study, it seems unlikely that Cherenkov light emission from these radiation sources is a suitable source for phototherapy.

One exception to the above is ^{90}Y, which may be used for radioembolization delivering doses on the order of 100 Gy, e.g. TheraSphere® treatment. In this case, the total light fluence can be calculated using Eq. (16), and is ~0.03 – 0.05 mJ/cm^2 in the presence of optical absorption and ~0.4 – 0.8 mJ/cm^2 in the absence of optical absorption between 250 – 850 nm. Given the similar fluence rates calculated for ^{90}Y with respect to the radiotherapy beams (see Figure 5), it is expected that electron and x-ray photon beams may also deliver a Cherenkov radiation fluence on the order of [mJ/cm^2] during external beam radiotherapy. The values for both radionuclides and radiotherapy beams could be calculated in a given waveband using the percentages in Table 3, and scaled by the refractive index factor presented in Figure 7.

Given the recent interest into low-light level phototherapy, these values may help in guiding the emerging applications using Cherenkov radiation as the light source (Farrell et al., 1998, Gonzales et al., 2014, Hartl et al., 2015, Kotagiri et al., 2015). Taken as a whole, the light levels from imaging radionuclides (e.g. ^{18}F) are many orders of magnitude lower than reported threshold values for photodynamic action, while Cherenkov radiation fluence levels from external beams and ^{90}Y are on the order of [mJ/cm^2] which may potentially be, albeit a weak, excitation source for phototherapy. Therefore it is not obvious that Cherenkov could be used as an efficient means to activate a phototherapeutic effect *in-vivo* without some

additional photochemistry (e.g., radiosensitization, scintillation or direct electron transfer reactions) also contributing to the process.

5. Conclusions

In recent years there has been a growing interest in biomedical applications of Cherenkov radiation from both radionuclides and external radiotherapy beams. To realize the potential of this emerging field, in this study the quantitative light fluence of Cherenkov radiation from these radiation sources has been estimated for the first time, which have the potential to help define detection limits, efficiencies, and ultimately the development of future biomedical applications utilizing Cherenkov radiation. These light intensities are low, and while useful, practical application will require highly sensitive imaging systems, or highly sensitive photochemistry alterations.

Acknowledgments

This study has been financially supported by Pilot Grant Funds from Norris Cotton Cancer Center, as well as NIH grants R21EB17559 and R01CA109558.

References

Agostinelli S, Allison J, Amako K, Apostolakis J, Araujo H, Arce P, Asai M, Axen D, Banerjee S, Barrand G, Behner F, Bellagamba L, Boudreau J, Broglia L, Brunengo A, Burkhardt H, Chauvie S, Chuma J, Chytracek R, Cooperman G, Cosmo G, Degtyarenko P, Dell'acqua A, Depaola G, Dietrich D, Enami R, Feliciello A, Ferguson C, Fesefeldt H, Folger G, Foppiano F, Forti A, Garelli S, Giani S, Giannitrapani R, Gibin D, Gómez Cadenas JJ, González I, Gracia Abril G, Greeniaus G, Greiner W, Grichine V, Grossheim A, Guatelli S, Gumplinger P, Hamatsu R, Hashimoto K, Hasui H, Heikkinen A, Howard A, Ivanchenko V, Johnson A, Jones FW, Kallenbach J, Kanaya N, Kawabata M, Kawabata Y, Kawaguti M, Kelner S, Kent P, Kimura A, Kodama T, Kokoulin R, Kossov M, Kurashige H, Lamanna E, Lampén T, Lara V, Lefebure V, Lei F, Liendl M, Lockman W, Longo F, Magni S, Maire M, Medernach E, Minamimoto K, Mora De Freitas P, Morita Y, Murakami K, Nagamatu M, Nartallo R, Nieminen P, Nishimura T, Ohtsubo K, Okamura M, O'neale S, Oohata Y, Paech K, Perl J, Pfeiffer A, Pia MG, Ranjard F, Rybin A, Sadilov S, Di Salvo E, Santin G, Sasaki T, Savvas N, Sawada Y, et al. Geant4—a simulation toolkit. Nuclear Instruments and Methods in Physics Research Section A: Accelerators, Spectrometers, Detectors and Associated Equipment. 2003; 506:250–303.

Arce, P.; Rato, P.; Canadas, M.; Lagares, J. IGAMOS: A Geant4-based easy and flexible framework for nuclear medicine applications. Nuclear Science Symposium Conference Record, 2008; NSS '08. IEEE; 19–25 Oct. 2008; 2008. p. 3162-3168.

Axelsson J, Davis SC, Gladstone DJ, Pogue BW. Cerenkov emission induced by external beam radiation stimulates molecular fluorescence. Med Phys. 2011; 38:4127–4132. [PubMed: 21859013]

Beattie BJ, Thorek DL, Schmidtlein CR, Pentlow KS, Humm JL, Hielscher AH. Quantitative modeling of Cerenkov light production efficiency from medical radionuclides. PLoS One. 2012; 7:e31402. [PubMed: 22363636]

Bevilacqua F, Berger AJ, Cerussi AE, Jakubowski D, Tromberg BJ. Broadband absorption spectroscopy in turbid media by combined frequency-domain and steady-state methods. Appl Opt. 2000; 39:6498–6507. [PubMed: 18354663]

Boschi F, Calderan L, D'ambrosio D, Marengo M, Fenzi A, Calandrino R, Sbarbati A, Spinelli AE. In vivo (1)(8)F-FDG tumour uptake measurements in small animals using Cerenkov radiation. Eur J Nucl Med Mol Imaging. 2011; 38:120–127. [PubMed: 20882278]

Carpenter CM, Ma X, Liu H, Sun C, Pratx G, Wang J, Gambhir SS, Xing L, Cheng Z. Cerenkov luminescence endoscopy: improved molecular sensitivity with beta--emitting radiotracers. J Nucl Med. 2014; 55:1905–1909. [PubMed: 25300598]

Čerenkov PA. The visible glow of pure liquid under the effect of hard γ-rays. Comptes Rendus De L Academie Des Sciences De L Urss. 1937; 14:101–105.

Cerussi AE, Berger AJ, Bevilacqua F, Shah N, Jakubowski D, Butler J, Holcombe RF, Tromberg BJ. Sources of absorption and scattering contrast for near-infrared optical mammography. Acad Radiol. 2001; 8:211–218. [PubMed: 11249084]

Durduran T, Choe R, Culver JP, Zubkov L, Holboke MJ, Giammarco J, Chance B, Yodh AG. Bulk optical properties of healthy female breast tissue. Phys Med Biol. 2002; 47:2847–2861. [PubMed: 12222850]

Farrell TJ, Wilson BC, Patterson MS, Olivo MC. Comparison of the in vivo photodynamic threshold dose for photofrin, mono- and tetrasulfonated aluminum phthalocyanine using a rat liver model. Photochem Photobiol. 1998; 68:394–399. [PubMed: 9747595]

Gill RK, Mitchell GS, Cherry SR. Computed Cerenkov luminescence yields for radionuclides used in biology and medicine. Phys Med Biol. 2015; 60:4263–4280. [PubMed: 25973972]

Glaser AK, Andreozzi JM, Davis SC, Zhang R, Pogue BW, Fox CJ, Gladstone DJ. Video-rate optical dosimetry and dynamic visualization of IMRT and VMAT treatment plans in water using Cherenkov radiation. Med Phys. 2014; 41:062102. [PubMed: 24877829]

Glaser AK, Davis SC, Mcclatchy DM, Zhang R, Pogue BW, Gladstone DJ. Projection imaging of photon beams by the Cerenkov effect. Med Phys. 2013a; 40:012101. [PubMed: 23298103]

Glaser AK, Davis SC, Voigt WH, Zhang R, Pogue BW, Gladstone DJ. Projection imaging of photon beams using Cerenkov-excited fluorescence. Phys Med Biol. 2013b; 58:601–619. [PubMed: 23318469]

Glaser AK, Kanick SC, Zhang R, Arce P, Pogue BW. A GAMOS plug-in for GEANT4 based Monte Carlo simulation of radiation-induced light transport in biological media. Biomed Opt Express. 2013c; 4:741–759. [PubMed: 23667790]

Glaser AK, Voigt WH, Davis SC, Zhang R, Gladstone DJ, Pogue BW. Three-dimensional Cerenkov tomography of energy deposition from ionizing radiation beams. Opt Lett. 2013d; 38:634–636. [PubMed: 23455248]

Glaser AK, Zhang R, Davis SC, Gladstone DJ, Pogue BW. Time-gated Cherenkov emission spectroscopy from linear accelerator irradiation of tissue phantoms. Opt Lett. 2012; 37:1193–1195. [PubMed: 22466192]

Gonzales J, Wang F, Zamora G, Trinidad A, Marcu L, Cherry S, Hirschberg H. Ultra low fluence rate photodynamic therapy: simulation of light emitted by the Cerenkov effect. 2014 89280F-89280F-11.

Hartl BA, Hirschberg H, Marcu L, Cherry SR. Characterizing low fluence thresholds for in vitro photodynamic therapy. Biomed Opt Express. 2015; 6:770–779. [PubMed: 25798302]

Holland JP, Normand G, Ruggiero A, Lewis JS, Grimm J. Intraoperative imaging of positron emission tomographic radiotracers using Cerenkov luminescence emissions. Mol Imaging. 2011; 10:177–186. 1–3. [PubMed: 21496448]

Hu Z, Liang J, Yang W, Fan W, Li C, Ma X, Chen X, Ma X, Li X, Qu X, Wang J, Cao F, Tian J. Experimental Cerenkov luminescence tomography of the mouse model with SPECT imaging validation. Opt Express. 2010; 18:24441–24450. [PubMed: 21164791]

Icrp. International Commission on Radiological Protection, Radiation Dose to Patients from Radiopharmaceuticals. 1988; 1–4

Jacques SL. Optical properties of biological tissues: a review. Phys Med Biol. 2013; 58:R37–R61. [PubMed: 23666068]

Jakubowski DB, Cerussi AE, Bevilacqua F, Shah N, Hsiang D, Butler J, Tromberg BJ. Monitoring neoadjuvant chemotherapy in breast cancer using quantitative diffuse optical spectroscopy: a case study. J Biomed Opt. 2004; 9:230–238. [PubMed: 14715078]

Jarvis LA, Zhang R, Gladstone DJ, Jiang S, Hitchcock W, Friedman OD, Glaser AK, Jermyn M, Pogue BW. Cherenkov Video Imaging Allows for the First Visualization of Radiation Therapy in Real Time. Int J Radiat Oncol Biol Phys. 2014

Kotagiri N, Sudlow GP, Akers WJ, Achilefu S. Breaking the depth dependency of phototherapy with Cerenkov radiation and low-radiance-responsive nanophotosensitizers. Nat Nanotechnol. 2015; 10:370–379. [PubMed: 25751304]

Kudo T, Fukuchi K, Annala AJ, Chatziioannou AF, Allada V, Dahlbom M, Tai YC, Inubushi M, Huang SC, Cherry SR, Phelps ME, Schelbert HR. Noninvasive measurement of myocardial activity concentrations and perfusion defect sizes in rats with a new small-animal positron emission tomograph. Circulation. 2002; 106:118–123. [PubMed: 12093780]

Li CQ, Mitchell GS, Cherry SR. Cerenkov luminescence tomography for small-animal imaging. Optics Letters. 2010; 35:1109–1111. [PubMed: 20364233]

Liu H, Carpenter CM, Jiang H, Pratx G, Sun C, Buchin MP, Gambhir SS, Xing L, Cheng Z. Intraoperative imaging of tumors using Cerenkov luminescence endoscopy: a feasibility experimental study. J Nucl Med. 2012; 53:1579–1584. [PubMed: 22904353]

Lohrmann C, Zhang H, Thorek DL, Desai P, Zanzonico PB, O'donoghue JA, Irwin CP, Reiner T, Grimm J, Weber WA. Cerenkov luminescence imaging for radiation dose calculation of a 90Y-labeled gastrin releasing peptide receptor (GRPr) antagonist. J Nucl Med. 2015

Mitchell GS, Gill RK, Boucher DL, Li C, Cherry SR. In vivo Cerenkov luminescence imaging: a new tool for molecular imaging. Philos Transact A Math Phys Eng Sci. 2011; 369:4605–4619.

Ran C, Zhang Z, Hooker J, Moore A. In vivo photoactivation without "light": use of Cherenkov radiation to overcome the penetration limit of light. Mol Imaging Biol. 2012; 14:156–162. [PubMed: 21538154]

Robertson R, Germanos MS, Li C, Mitchell GS, Cherry SR, Silva MD. Optical imaging of Cerenkov light generation from positron-emitting radiotracers. Phys Med Biol. 2009; 54:N355–N365. [PubMed: 19636082]

Sandell JL, Zhu TC. A review of in-vivo optical properties of human tissues and its impact on PDT. J Biophotonics. 2011; 4:773–787. [PubMed: 22167862]

Spinelli AE, D'ambrosio D, Calderan L, Marengo M, Sbarbati A, Boschi F. Cerenkov radiation allows in vivo optical imaging of positron emitting radiotracers. Phys Med Biol. 2010; 55:483–495. [PubMed: 20023328]

Spinelli L, Torricelli A, Pifferi A, Taroni P, Danesini GM, Cubeddu R. Bulk optical properties and tissue components in the female breast from multiwavelength time-resolved optical mammography. J Biomed Opt. 2004; 9:1137–1142. [PubMed: 15568933]

Thorek DL, Abou DS, Beattie BJ, Bartlett RM, Huang R, Zanzonico PB, Grimm J. Positron lymphography: multimodal, high-resolution, dynamic mapping and resection of lymph nodes after intradermal injection of 18F-FDG. J Nucl Med. 2012; 53:1438–1445. [PubMed: 22872741]

Thorek DL, Riedl CC, Grimm J. Clinical Cerenkov luminescence imaging of (18)F-FDG. J Nucl Med. 2014; 55:95–98. [PubMed: 24078721]

Tromberg BJ, Coquoz O, Fishkin JB, Pham T, Anderson ER, Butler J, Cahn M, Gross JD, Venugopalan V, Pham D. Non-invasive measurements of breast tissue optical properties using frequency-domain photon migration. Philos Trans R Soc Lond B Biol Sci. 1997; 352:661–668. [PubMed: 9232853]

Zhang R, Fox CJ, Glaser AK, Gladstone DJ, Pogue BW. Superficial dosimetry imaging of Cerenkov emission in electron beam radiotherapy of phantoms. Phys Med Biol. 2013a; 58:5477–5493. [PubMed: 23880473]

Zhang R, Gladstone DJ, Jarvis LA, Strawbridge RR, Jack Hoopes P, Friedman OD, Glaser AK, Pogue BW. Real-time in vivo Cherenkoscopy imaging during external beam radiation therapy. J Biomed Opt. 2013b; 18:110504. [PubMed: 24247743]

Zhang R, Glaser AK, Gladstone DJ, Fox CJ, Pogue BW. Superficial dosimetry imaging based on Cerenkov emission for external beam radiotherapy with megavoltage x-ray beam. Med Phys. 2013c; 40:101914. [PubMed: 24089916]

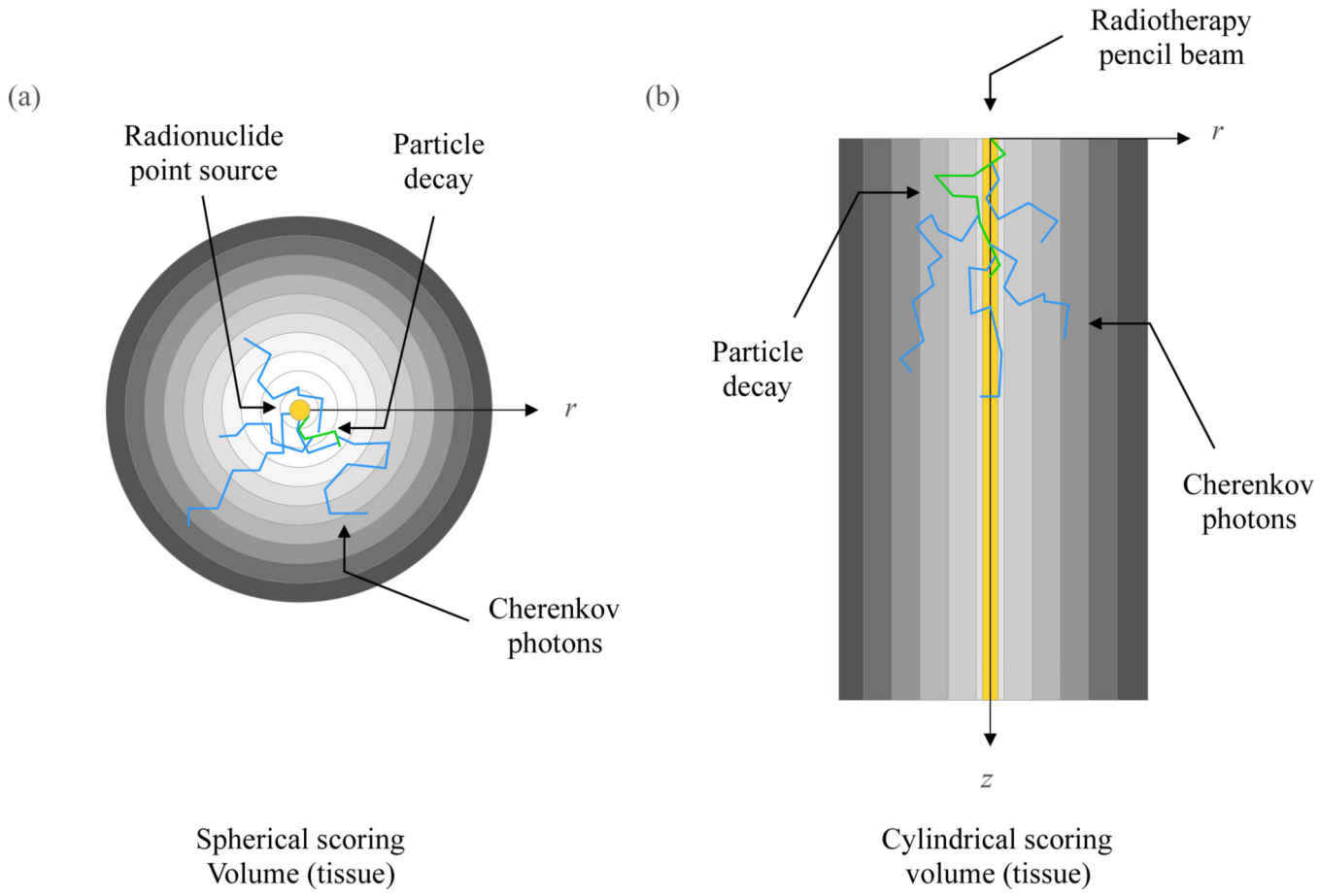

Figure 1.

In (a) the simulation geometry for the radionuclides is shown. All particle decays (green) are initiated at the origin, and the fluence of the induced Cherenkov radiation (blue) is recorded as a function or radius, *r*, in spherical shells. In (b) the simulation geometry for the radiotherapy beams is shown. All particles (green) are initiated at the origin and downward along the *z* axis. The fluence of the induced Cherenkov radiation (blue) is recorded as a function of radius, *r*, and depth, *z*. (color online).

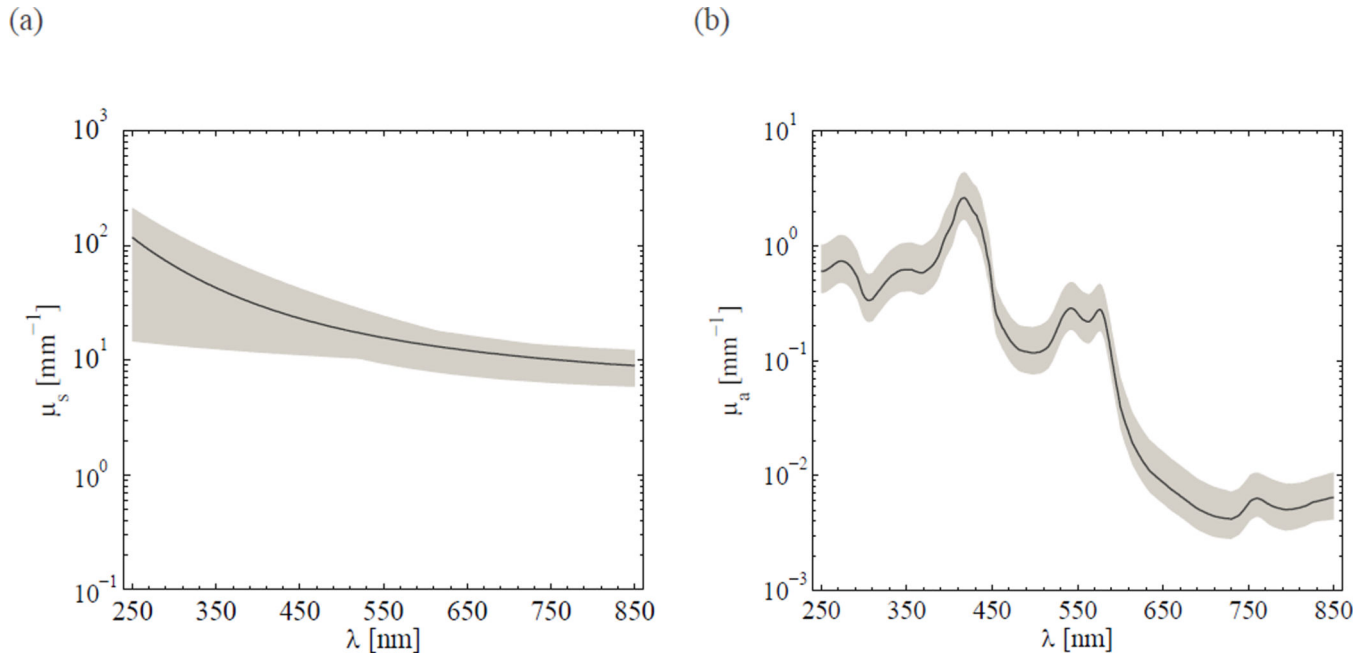

Figure 2.

In (a) the optical scattering coefficient, μ_s, is plotted. The median value (solid line) as well as minimum and maximum values (shaded region) as a function of wavelength of all optical property combinations are shown. In (b) the optical absorption coefficient, μ_a, is shown.

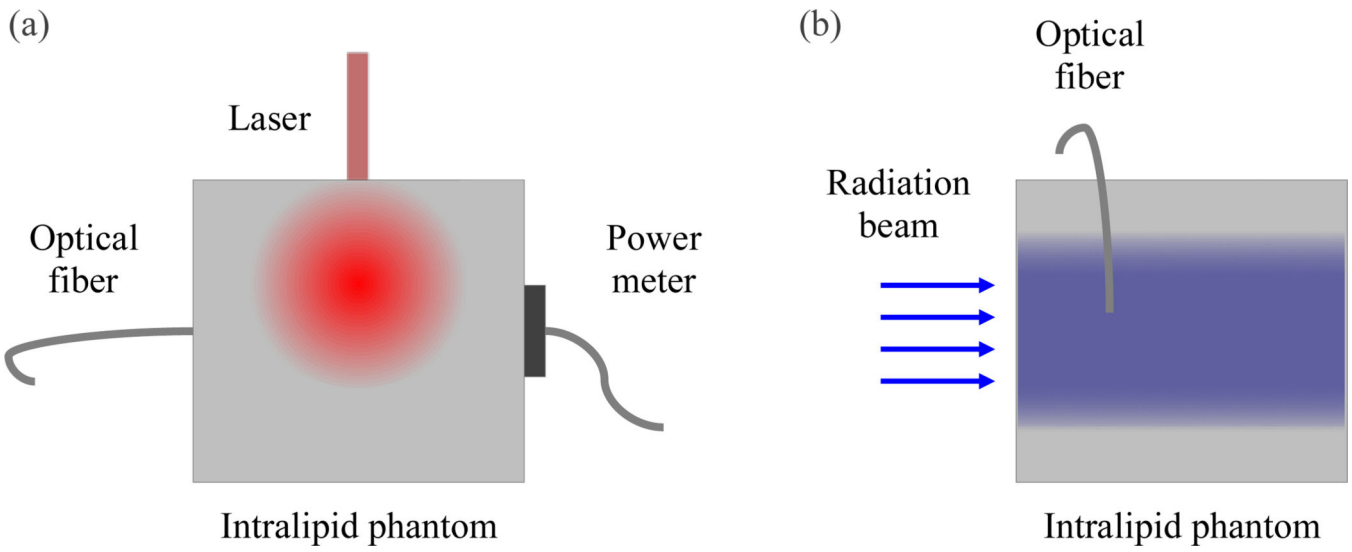

Figure 3.

In (a) the experimental geometry for determining the conversion factor from [counts/sec] collected by the optical fiber to [W/cm^2] collected by the power meter from a laser source is shown. In (b) the geometry for measuring the [counts/sec] with an optical fiber from an external 6 MV x-ray photon radiation beam is shown.

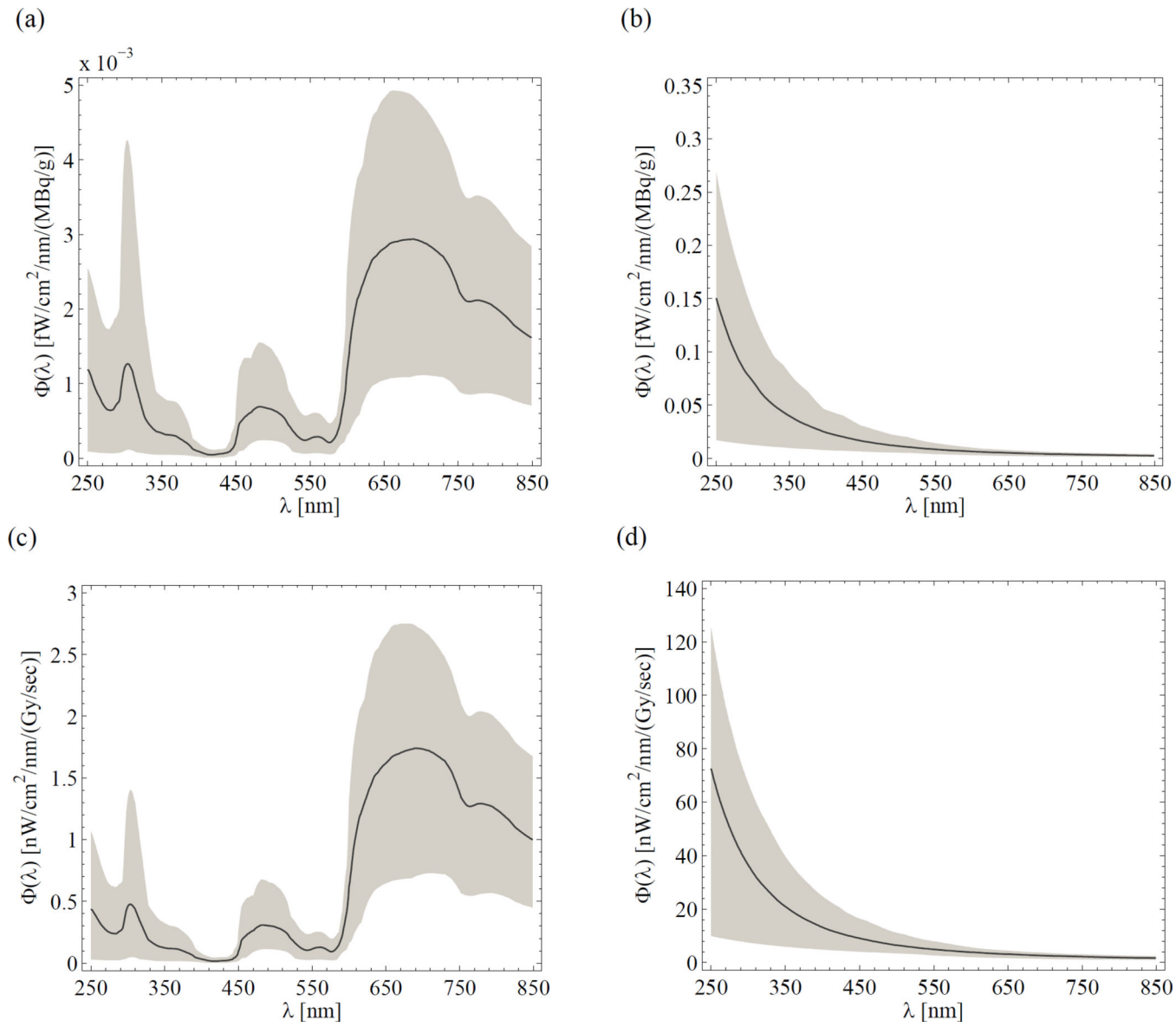

Figure 4.

In (a) and (b) the fluence rate, Φ, from ^{18}F for the various optical property combinations with and without optical absorption are shown respectively. In (c) and (d) the fluence rate, Φ, for a 6 MV x-ray photon beam is shown. In all plots, the median fluence rate (solid line) and maximum and minimum range for all optical property combinations (shaded region) are depicted.

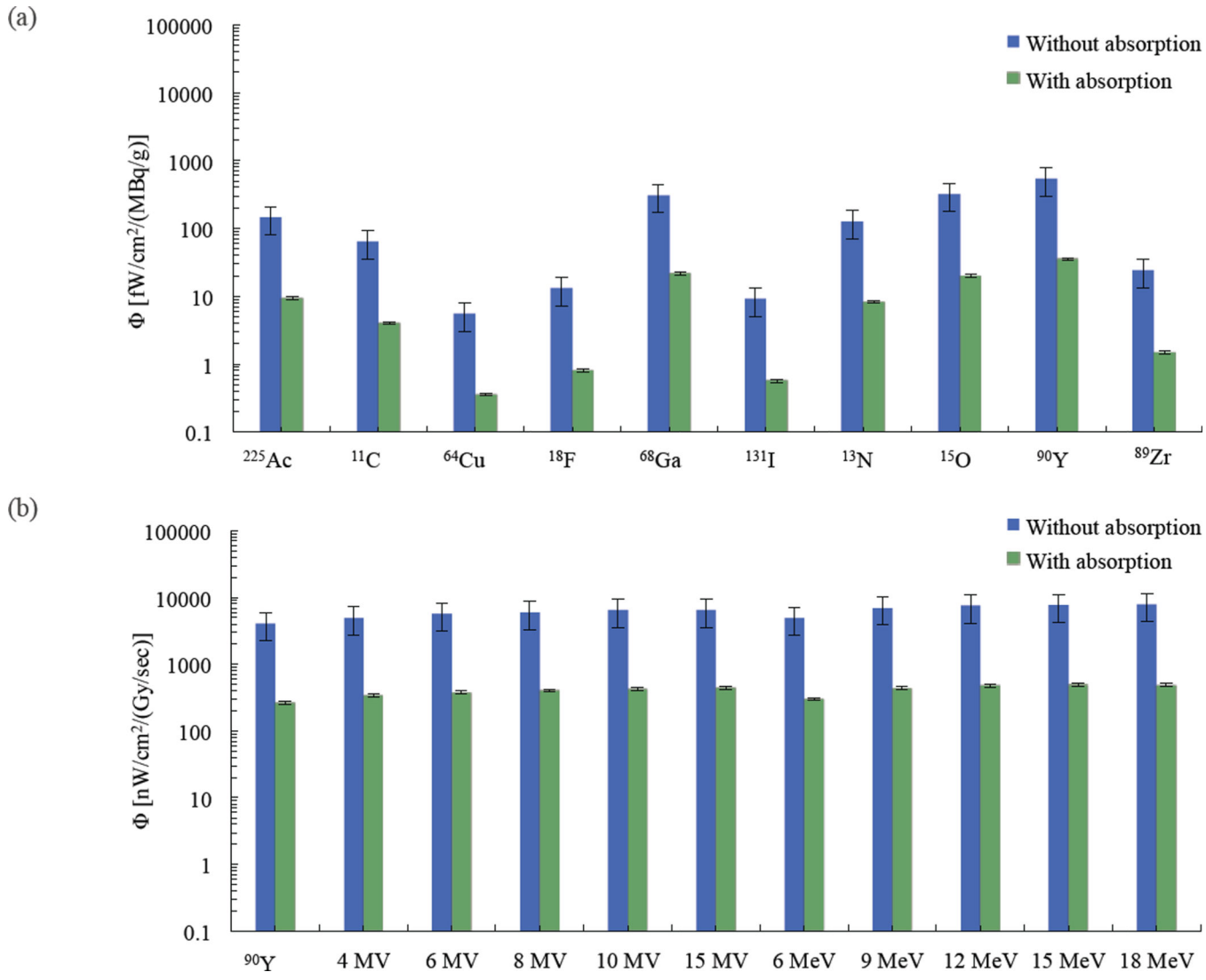

Figure 5.

In (a) and (b) the fluence rate, Φ, from ^{18}F for the various optical property combinations with and without optical absorption are shown respectively. In (c) and (d) the fluence rate, Φ, for a 6 MV x-ray photon beam is shown. In all plots, the median fluence rate (solid line) and maximum and minimum range for all optical property combinations (shaded region) are depicted.

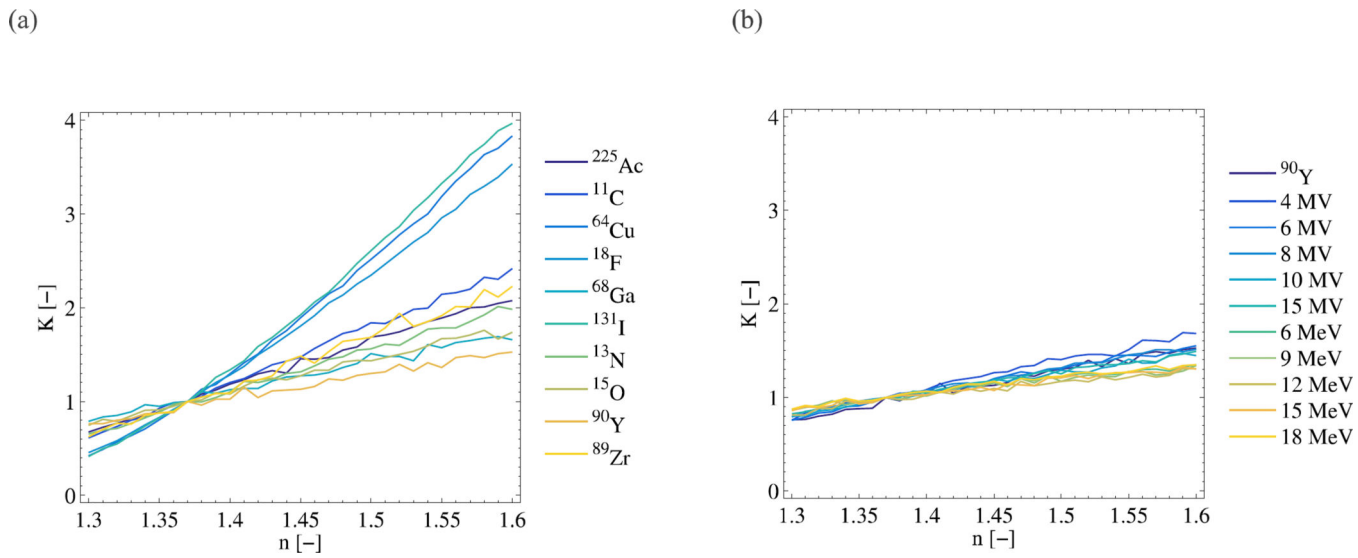

Figure 6.

In (a) and (b) the refractive index factor, *K*, is plotted for all radionuclides and external radiotherapy beams respectively. The factor K is normalized to a value of 1.0 at a refractive index of $n = 1.37$.

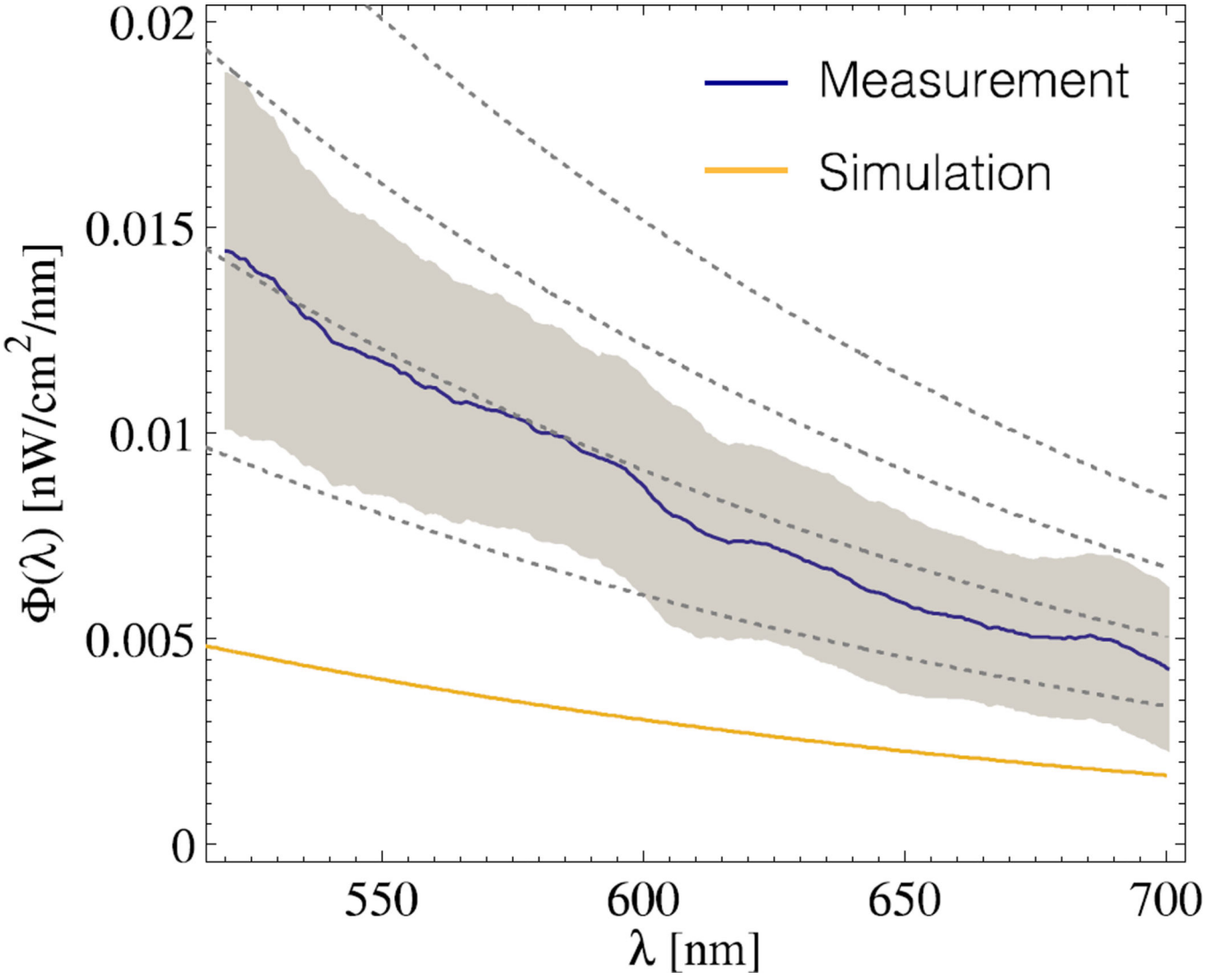

Figure 7.

The fluence rate, Φ, from a 6 MV external radiotherapy beam in a 1% v/v phantom of Intralipid. The measurement and uncertainties are shown in (black) and (shaded grey). The predicted fluence rate from the Monte Carlo simulations is shown in (blue).

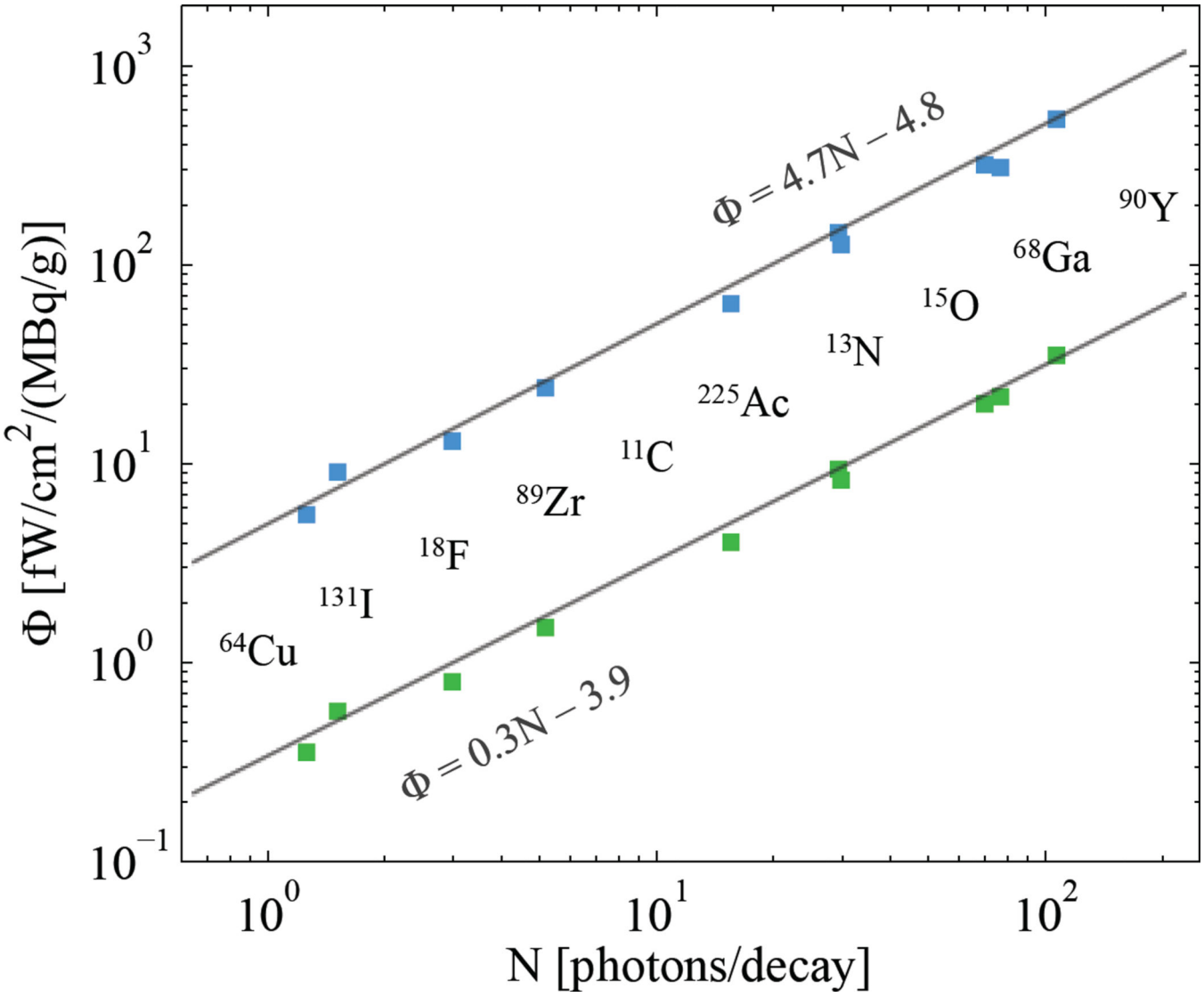

Figure 8.

The results of Gill *et. al.* for the radionuclides examined in this study are shown in units of [photons/decay] on the x-axis against the fluence rate estimates in this study with absorption (green) and without absorption (blue). The linear fitting lines for both are shown.

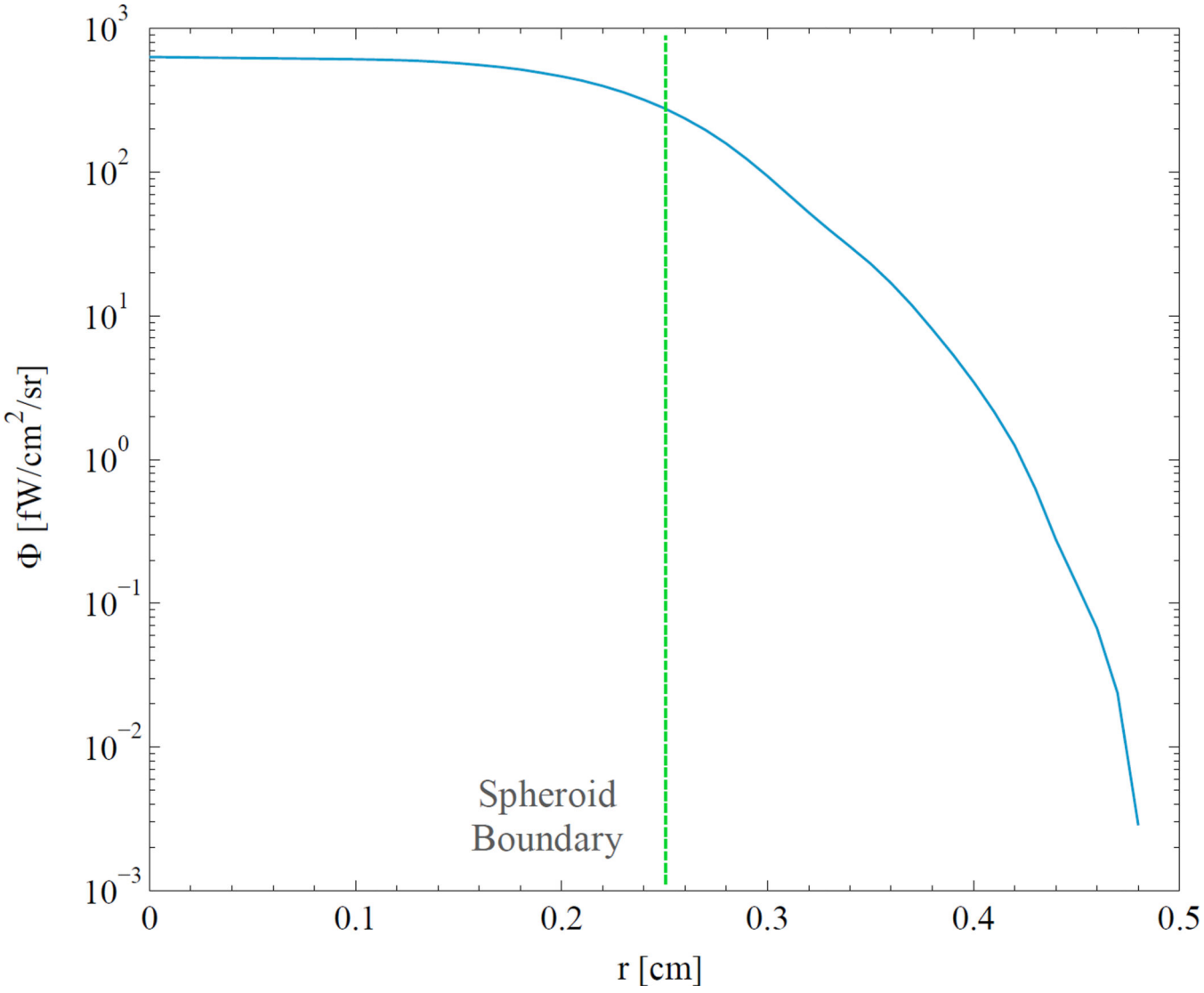

Figure 9.

The fluence rate as a function of radial distance, *r*, is plotted for a uniformly distributed spheroid of ^{90}Y of radius 0.25 cm and tissue tracer concentration of 0.003 MBq/g between 400 – 800 nm averaged across all of the optical properties combinations used in this study (including absorption).

Table 1

Parameters of the scattering coefficient for breast tissue.

a [mm^{-1}]	f_{Ray}[arb u.]	b_{Mie}[arb u.]	Tissue	Reference
3.18	0.00	2.741	Breast	(Sandell and Zhu, 2011)
1.52	0.58	0.000	Breast	(Sandell and Zhu, 2011)
2.48	0.00	1.544	Breast	(Sandell and Zhu, 2011)
2.02	0.18	0.638	Breast	(Sandell and Zhu, 2011)
1.81	0.41	0.000	Breast	(Spinelli et al., 2004)
1.74	0.60	0.076	Breast, premenopausal	(Cerussi et al., 2001)
1.11	0.54	0.009	Breast, postmenopausal	(Cerussi et al., 2001)
1.05	0.00	0.473	Breast	(Durduran et al., 2002)

Table 2

Parameters of the absorption coefficient for breast tissue.

C_{HGb} [μM]	B [%]	S [%]	W [%]	F [%]	Tissue	Reference
23.6	1.02	67.6	14.4	65.6	Breast, normal	(Tromberg et al., 1997)
24.2	1.04	75.5	29.2	51.7	Breast, normal	(Bevilacqua et al., 2000)
16.0	0.69	62.6	6.0	74.0	Breast, normal	(Jakubowski et al., 2004)
15.7	0.67	66.4	14.5	58.0	Breast, normal	(Spinelli et al., 2004)
41.0	1.76	61.1	41.0	39.0	Breast, tumor	(Jakubowski et al., 2004)

Table 3

Relative spectral components of the Cherenkov radiation fluence.

	Wavelength ranges [nm]					
	250–350	**350–450**	**450–550**	**550–650**	**650–750**	**750–850**
With absorption [%]	8.8 +/− 2.2	1.8 +/− 0.4	5.2 +/− 0.8	16.4 +/− 0.3	39.0 +/− 1.9	28.8 +/− 1.6
Without absorption [%]	57.7 +/− 2.4	19.5 +/− 0.6	9.7 +/− 0.6	5.9 +/− 0.5	4.1 +/− 0.4	3.1 +/− 0.3